LBL-8512 c. 2
Preprint

Lawrence Berkeley Laboratory
UNIVERSITY OF CALIFORNIA, BERKELEY, CA

Submitted to Zietschrift fur Physik

A THEORETICAL INVESTIGATION OF SHELL EFFECTS IN DEEP INELASTIC COLLISIONS

L. G. Sobotka, G. J. Mathews, and L. G. Moretto

May 1979

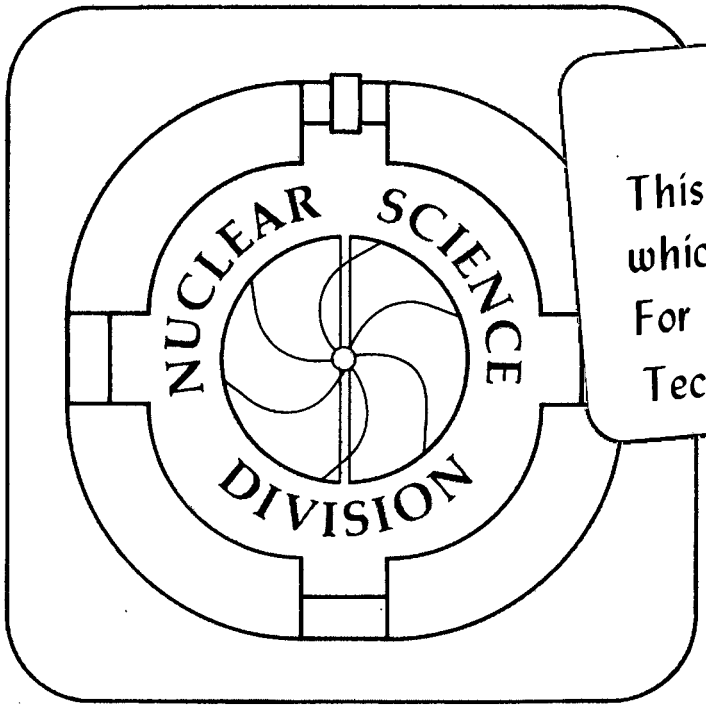

Prepared for the U. S. Department of Energy
under Contract W-7405-ENG-48

DISCLAIMER

LBL-8512

A THEORETICAL INVESTIGATION OF SHELL EFFECTS IN DEEP INELASTIC COLLISIONS

L. G. Sobotka, G. J. Mathews, and L. G. Moretto

Lawrence Berkeley Laboratory
University of California
Berkeley, California 94720

ABSTRACT

The relative importance of three different influences of independent-particle shell structure on the nucleon transport process during heavy-ion collisions are discussed. Results of calculations for the 620-MeV $^{86}Kr + ^{197}Au$ system are presented.

I. INTRODUCTION

The importance of shell effects in the product mass distribution from two interacting, relatively low-energy, nuclei is well known in fission. These shell effects are also known to persist up to fairly high (~40 MeV) excitation energies for the fissioning system. In this work we have taken steps toward the incorporation of this well known feature into another system of two interacting nuclei, namely, the nucleon transport (diffusion) process [1,2] associated with heavy-ion collisions. The effects of shell structure on the mass transport coefficients have been investigated schematically by Schurmann, Nörenberg, and Simbel [3] in the framework of the quantum statistical theory of Nörenberg [2]. In this work we consider the influence of shell structure in more detail and in the framework of transition probabilities based upon the level densities of the system [1,4].

Shell effects manifest themselves in the diffusion process in three ways. The most important effect is from the potential energy of the system as a function of asymmetry. This potential-energy surface, calculated according to the Strutinsky procedure [5], is described in Section II. Shell effects are also manifested in the statistical level density of the ion-ion complex and the moments of inertia for the colliding nuclei. These effects are also described in Section II. In Section III results are discussed from a diffusion calculation based on a simplified picture of the ion-ion complex as two overlapping spheres.

II. THE MODEL

1. The Diffusion Model

The entire formulation of the stochastic transport process is summarized in the master equation [1]

$$\dot{\phi}_z(t) = \sum_{z'=z\pm1} (\Lambda_{z',z}\phi_{z'}(t) - \Lambda_{zz'}\phi_z(t)) \quad , \tag{1}$$

where $\phi_z(t)$ is the relative population of the asymmetry z at time t, and $\Lambda_{zz'}$ is the macroscopic transition probability for the system to change asymmetry from z to z'.

The influence of shell effects is manifested in the transition probabilities. If the statistical approach is valid, one can apply the Fermi golden rule to write

$$\Lambda_{zz'} = \lambda_{zz'}\, \rho_{z'}(E - V_{z'}) \quad , \tag{2}$$

where $\lambda_{zz'}$ is a microscopic transition probability and the level density, $\rho_{z'}(E-V_{z'})$, simply counts the statistical weight for the system to find itself in the final asymmetry, z'. The most important effect of shell structure is immediately obvious at this point. At a fixed total energy for the system, E, hills and valleys in the potential energy as a function of asymmetry will cause drastic changes in the level density from one z to the next, hence driving the system toward higher populations in the vicinity of valleys.

Of course a solution to Eq. (1) will require the specification of the microscopic transition probabilities, $\lambda_{zz'}$. These we take as,

$$\lambda_{zz'} = \frac{2\kappa f}{(\rho_z(E-V_z) + \rho_{z'}(E-V_{z'}))} \tag{3}$$

which obeys microscopic reversibility and therefore guarantees that the system will obtain the correct equilibrium limit. A theoretical justification for this form of $\lambda_{zz'}$ is given in Ref. [4]. The factors in the numerator are an average transition flux, κ, and a form factor, f. These quantities we take from the one-body proximity formulation [6,7].

2. The Strutinski Correction

As we shall see in Section III, the most important influence of shell effects on nucleon transport stems from the potential energy surface as a function of asymmetry. For this calculation we have employed the well known Strutinsky procedure [5]. The details of the calculation, which we have done including the parametrization of the single-particle potential and the pairing strength as a function of asymmetry, are described in the work of Nilsson et al. [8]. The only modification introduced here is a technical one. When needed, we have modified the BCS configuration space from the $\pm\sqrt{15n}$ levels from the last occupied level (where n is the number of particles)used in Ref. [8] so that shell corrections can be made for nuclei with fewer than $\sqrt{15n}$ levels below the last occupied level. To avoid any spurious discontinuity in the pairing potential, Δ, we renormalize the pairing strength G to a value which would yield the same value for Δ as the $\sqrt{15n}$ range in the equidistant model, i.e., we let $G = G_o/(1 - G_o\, g\, \ell n\, \sqrt{15n}/\omega)$,

where g is the average single-particle level spacing, G_o is the pairing strength from the Nilsson prescription, and ω is the number of levels below the last occupied level.

Figure 1 shows a two-dimensional contour of the shell correction in the asymmetry (labelled by the Z of one fragment assuming N/Z equilibrium) vs ε_2 (deformation of both fragments) plane for the $^{86}_{36}Kr + ^{197}_{79}Au$ system. We see that the shell effects are quite sizable (~±10 MeV for ε_2=0) for $\varepsilon_2 \lesssim 0.1$.

3. The Level Densities

A feature which tends to oppose the effect of the shell corrections to the potential energy surface is the influence of the single particle structure on the level density for a given nucleus. This we calculate for each fragment according to the statistical procedure outlined by Moretto et al.[9,10] We use the same shell model and pairing parameters as in the potential energy calculation. The total level density at a given asymmetry is then simply given by

$$\rho_Z(E-V_Z) = \int_0^{E-V_Z} \rho_1(E-V_Z-\varepsilon)\rho_2(\varepsilon)d\varepsilon = \rho_1(E_1^*)\rho_2(E_2^*) \times \int e^{-(\varepsilon-\varepsilon_o)^2/2\sigma^2} dE$$

$$= \sqrt{2\pi}\ \sigma\ \rho_1(E_1^*)\rho_2(E_2^*) \qquad (4)$$

where E_1^* and E_2^* are determined by assuming complete thermalization between the fragments. We neglect the slowly varying dependence of σ on E. In Fig. 2 we plot the total level density vs. asymmetry

for spherical fragments at several constant temperatures, again for $^{86}_{36}Kr + ^{197}_{79}Au$. Here we see, as intuitively expected, that the effect of shell closure is to significantly decrease the level density at a constant temperature. This effect, however, is more than compensated for in the calculations at fixed total energy by the increase in level density with the increase in the excitation energy (or temperature) which accompanies a valley in the potential energy surface. Nevertheless, the importance of this effect is clear in Fig. 2.

4. The Moments of Inertia and the Total Effective Potential

A third influence of shell structure on the transport process is a dynamical effect which stems from the relation between the single-particle structure and the moments of inertia of the colliding nuclei. These moments of inertia are also derived naturally from statistical theory [10]. A very transparent way to appreciate the influence of shell structure on the moment of inertia of a nucleus is in the equidistant model which gives [11],

$$\mathcal{I} = g\langle m^2 \rangle \hbar^2 \quad , \tag{5}$$

where m is the single-particle projection of angular momentum. Clearly two effects come into play. One is that near a closed shell the single-particle level density decreases so that the moment of inertia diminishes. At the same time the moment of inertia will increase or decrease depending upon the angular momenta of single-particle states near the Fermi energy.

In Fig. 3 we show moments of inertia relative to the rigid body ($\mathcal{I} = 2/5\ MR^2$) inertias calculated from the statistical model of Ref. [10]. In these calculations we have neglected the effect of pairing on the moment of inertia since this effect would, to some extent, have vanished for the angular momenta involved here. In the diffusion calculations the ratios in Fig. 3 were normalized to unity at the high temperature limit to compensate for the tendency [12] of the Nilsson single-particle levels to systematically produce moments of inertia which are too high.

The moments of inertia enter the transport process through the dependence of the effective potential energy surface on the rotational energy. The total effective potential energy of the system we take as

$$V_Z = \mathcal{U}(Z_1,A_1) + \mathcal{U}(Z_2,A_2) + Z_1Z_2e^2/r + U_{prox} + E_{rot} \quad , \qquad (6)$$

where $\mathcal{U}$ is the Strutinsky corrected droplet-model binding energy, U_{prox} is the proximity potential at a separation r, and E_{rot} is the rotational energy of the system,

$$E_{rot} = \ell^2\hbar^2/2\mu r^2 + \ell_1^2\hbar^2/2\mathcal{I}_1 + \ell_2^2\hbar^2/2\mathcal{I}_2 \quad . \qquad (7)$$

In the rigid rotation limit, E_{rot} becomes

$$E_{rot} = \hbar^2\ell_o^2/2(\mu r^2 + \mathcal{I}_1 + \mathcal{I}_2) \quad . \qquad (8)$$

It is clear from Eq. (8) that decreasing (increasing) moments of inertia should increase (decrease) the rotational energy and therefore hinder (favor) the transport process.

The final effective potential energy surface (calculated according to the method described in the next section) for 620-MeV $^{86}Kr + ^{197}Au$ at $\ell_{rms} = 220\ \hbar$ is shown in Fig. 4. Here it is clear that both the Strutinsky renormalization and the rotational inertias produce significant deviations from the smooth potential. This demonstrates the importance of including both of these effects in the transport calculation.

III. RESULTS

The calculations described in this section are based on a rather simplified picture of the ion-ion complex as two overlapping, rigidly rotating spheres, and because of this are to be taken only as a preliminary indication of a more rigorous treatment of the problem. Nevertheless, this picture probably is reasonable for the highest ℓ-waves where deformation effects are relatively unimportant and most of the cross section is weighted. As another argument in favor of the validity of the two spheres approximation, recall that the fission process, which although involving extreme deformations, is still well known to be sensitive to the shell structure at the scission point (~two touching spheres).

The calculations proceeded as follows. First, the Strutinsky calculation was performed for nuclei along the valley of N/Z equilibrium. Then level densities and moments of inertia were generated for these nuclei as a function of excitation energy, E*. The lifetime of the interaction and an average overlap of the two fragments was generated by a numerical integration of the equations of motion for the entrance

channel asymmetry under the influence of the proximity potential [13] and one-body dissipation [6]. Then by assuming rigid rotation, complete energy damping of radial kinetic energy, and thermal equilibrium between the fragments, unique values of $(E\text{-}V_Z) = E_1^* + E_2^*$, $E_{rot}(\ell_o)$, and $\rho_Z(E\text{-}V_Z)$ could be assigned at each asymmetry for each ℓ wave. Finally, the master equation (1) was solved numerically and the final populations were weighted according to impact parameter to obtain a cross section for the yield of each product Z.

The final populations of some representative ℓ-waves computed with and without shell effects for 620-MeV $^{86}Kr + ^{197}Au$ are shown in Fig. 5. The lifetimes indicated are from the numerical solution to the equations of motion and correspond to the lifetime in and out from the interaction radius ($R_o = r_1 + r_2 + 3.2$ fm). For orientation, ℓ_{max} for this reaction is about 310 $\hbar$. For ℓ = 270 $\hbar$, the effects of shell structure are seen to be relatively unimportant due to the short diffusion lifetime. However for the lower ℓ-waves a surprisingly dramatic influence from the N ~ 50 (Z_1 = 34) closed shell is obtained along with a wealth of finer structure. By comparing the ℓ = 220 $\hbar$ distribution with the effective potential energy in Fig. 4 one can clearly see the tendency of the shell effects to increase the population in the vicinity of valleys indicating the importance of the fluctuations in the potential energy surface. Further, one can conclude from Fig. 5 that shell effects may be most pronounced for lower ℓ-waves for which the system has more time to sample the potential.

In Fig. 6 the final angle-integrated Z-distribution is plotted and compared with the experimental data [14] and calculations which do not include shell corrections. The inclusion of shell effects improves the calculation for Z less than the projectile by adding cross section to this region, nevertheless, both the calculation with shell effects and the no-shell-effects charge distribution tend to overestimate the drift toward symmetry. This perhaps indicates a shortcoming of the two-spheres liquid-drop potential-energy surface employed here. This could of course be remedied by adjusting parameters, but that is beyond the scope of the present work which has been to demonstrate the relative importance of various shell effects on the mass transport process. This influence is clearly evident in Figs. 5 and 6. Of course to some extent the jagged structure, including the secondary peak at Z = 34 (N = 50), will be smoothed out when the N and Z degrees of freedom are allowed to relax independently and the fragments are allowed to deform. Also, some smoothing can be expected from charged particle evaporation after fragment separation so that one need not be surprised that the data do not exhibit the jagged structure of the calculations.

IV. CONCLUSION

In this work we have examined the possible role of shell effects on the mass transport process associated with deep-inelastic collisions. We have seen that such shell effects enter through the dependence of the transport on the system level density and are manifested in three ways. One way is through the corrections to the binding energy of the system, another is in the moment of inertia of the fragments, and the third is the level density itself. We have investigated the relative contribution of each of these terms on the transport process in the framework of a schematic picture of the ion-ion complex as two overlapping spheres constrained to have N/Z equilibrium. The conclusion of this work is that all three of these effects strongly influence the transition probabilities and therefore serious consideration should be given to each of them in any theory of shell effects in the nucleon transport process. However, in the case studied here it is not altogether clear what role, if any, the shell effects have played in the final experimental charge distribution. In future work a more detailed investigation of this role is planned in which the effects of

(N/Z) dispersion along with fragment deformation and neck formation will be taken into account. Also planned is a detailed investigation of possible experimental signatures of these shell effects.

Acknowledgments

The authors wish to acknowledge contributions of A. N. Behkami during the early phases of this work.

This work was supported by the Nuclear Physics Division of the U.S. Department of Energy.

1. Moretto,L.G. and Sventek,J.S., Phys. Lett. 58B, 26 (1975).
2. Nörenberg,W., Z. Physik A274, 241 (1975); A276, 84 (1976).
3. Schürmann,B., Nörenberg,W., and Simbel,M., Z.Physik A286, 263 (1978).
4. Barette,J. and Brau-Munzinger.P., Nucl. Phys. A287, 195 (1977).
5. Strutinsky,V.M., Nucl. Phys. A95, 420 (1967), and A122, 1 (1968).
6. Randrup,J., Ann. Phys. 112, 356 (1978).
7. Moretto,L.G., Symposium on the Macroscopic Features of Heavy-Ion Collisions and the Pre-equilibrium Process, Hakone, Japan (1977).
8. Nilsson,S.G., Tsang,C.F., Sobiczewski,A., Szymański, Z., Wycech,S., Gustafson,C., Lamm,I.L., Möller,P., Nilsson,B., Nucl. Phys. A 131, 1 (1969).
9. Moretto,L.G., Stella,R., and Caramella-Crespi,V., Energia Nucleare 17, 436 (1970).
10. Moretto,L.G., Nucl. Phys. A216, 1 (1973).
11. Ericson,T., Advan. Phys. 9, 425 (1960).
12. Andersson,G., Larsson,S.E., Leander,G., Möller,P., Nilsson,S.G., Ragnarsson,I., Åberg,S., Bengtsson,R., Dudek,J., Nerlo-Pomorska,B., Pomorski,K., Szymański,Z., Nucl. Phys. A 268, 205 (1976).
13. Blocki,J.P., Randrup,J., Swiatecki,W.J., and Tsang,C.F., Ann. Phys. 105, 427 (1977).
14. Russo,P., Schmitt,R.P., Wozniak,G.J., Jared,R.C., Glässel,P., Cauvin,B., Sventek,J.S., and Moretto,L.G., Nucl. Phys. A281, 509 (1977).

FIGURE CAPTIONS

Fig. 1. Shell correction contours in the asymmetry (Z) vs. deformation (ε_2) plane for the $^{86}_{36}Kr + ^{197}_{79}Au$ system.

Fig. 2. Total level density vs. asymmetry at several temperatures for the $^{38}_{36}Kr + ^{197}_{79}Au$ system.

Fig. 3. The ratio of the moment of inertia to the spherical liquid drop ($2/5\ MR^2$) inertia at different temperatures for nuclei along N/Z equilibrium for $^{86}Kr + ^{197}Au$.

Fig. 4. Total effective potential energy with (—) and without (--) shell effects as a function of asymmetry for the $^{86}_{36}Kr + ^{197}_{79}Au$ system at $\ell = 220\hbar = \ell_{rms}$, (a). The Strutinsky corrections, (b). The rotational energies, (c). We have assumed (N/Z) equilibrium, thermal equilibrium, and rigid rotation.

Fig. 5. Final populations, ϕ_Z, at several ℓ-waves for the 620-MeV $^{86}Kr + ^{197}Au$ reaction.

Fig. 6. Experimental (._._.) and calculated, with (—) and without (---) shell effects, total angle-integrated charge distributions for the 620-MeV $^{86}Kr + ^{197}Au$ reaction.

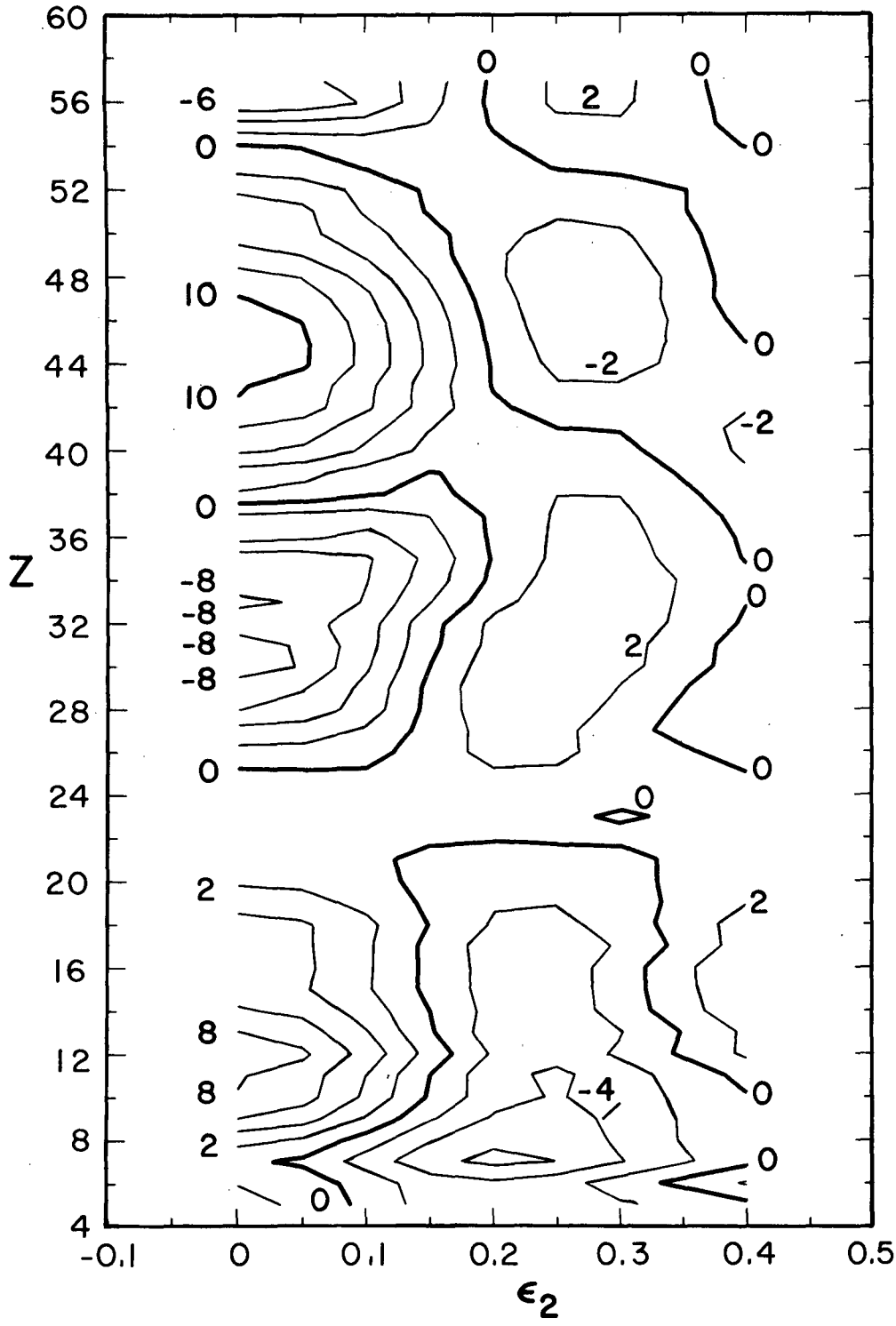

XBL 793-798

Fig. 1

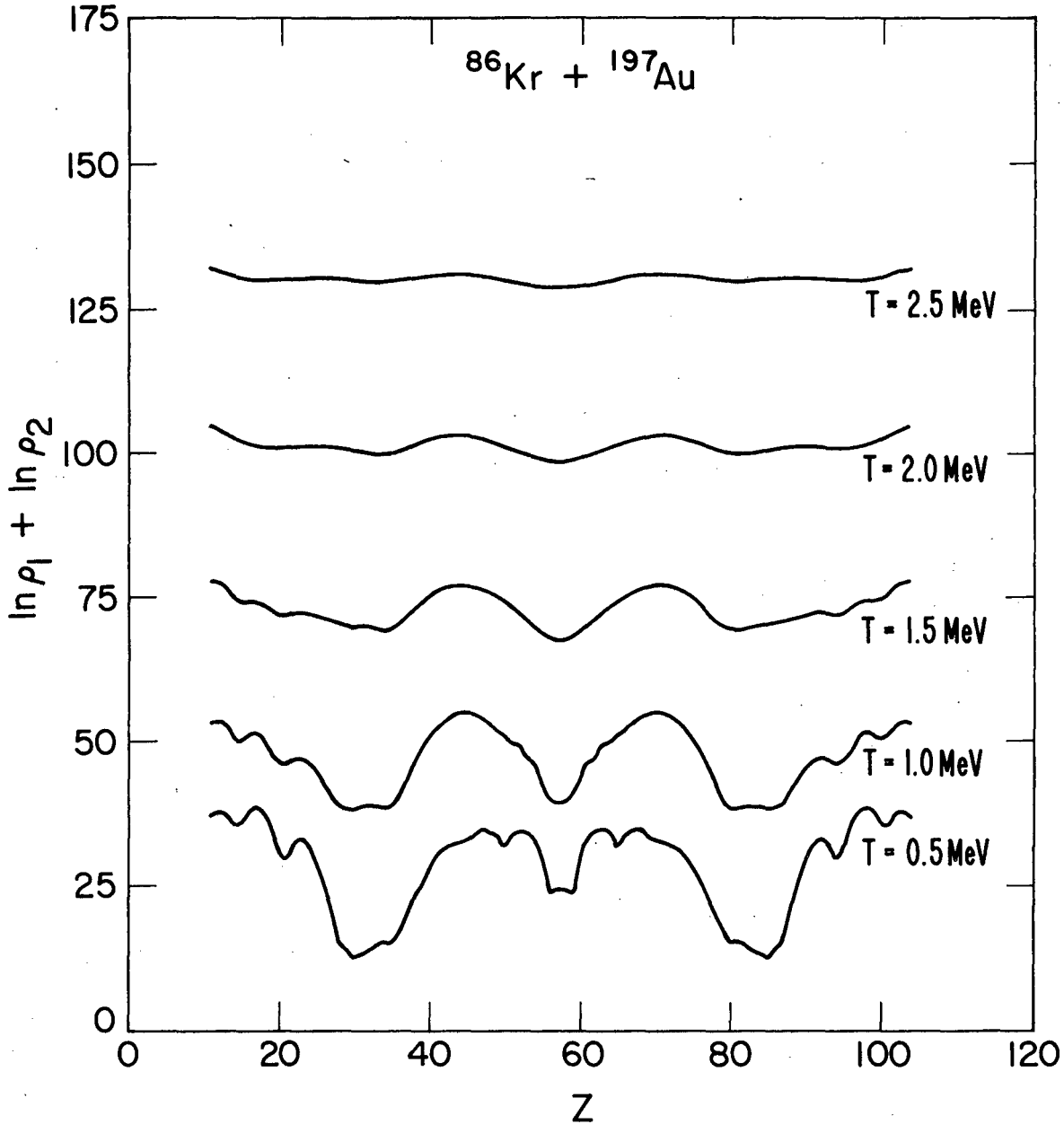

XBL 794-1330

Fig. 2

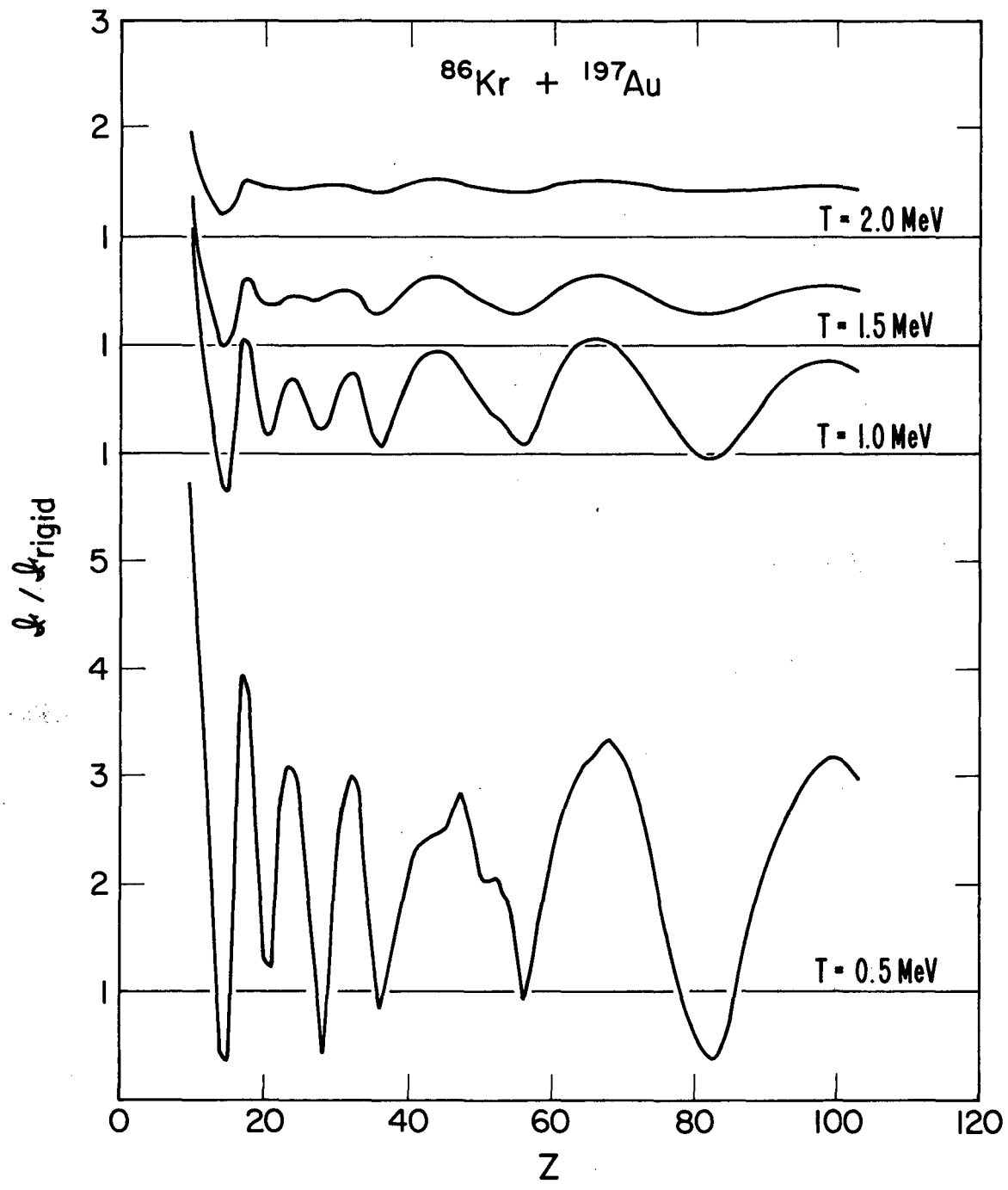

XBL 794-1331

Fig. 3

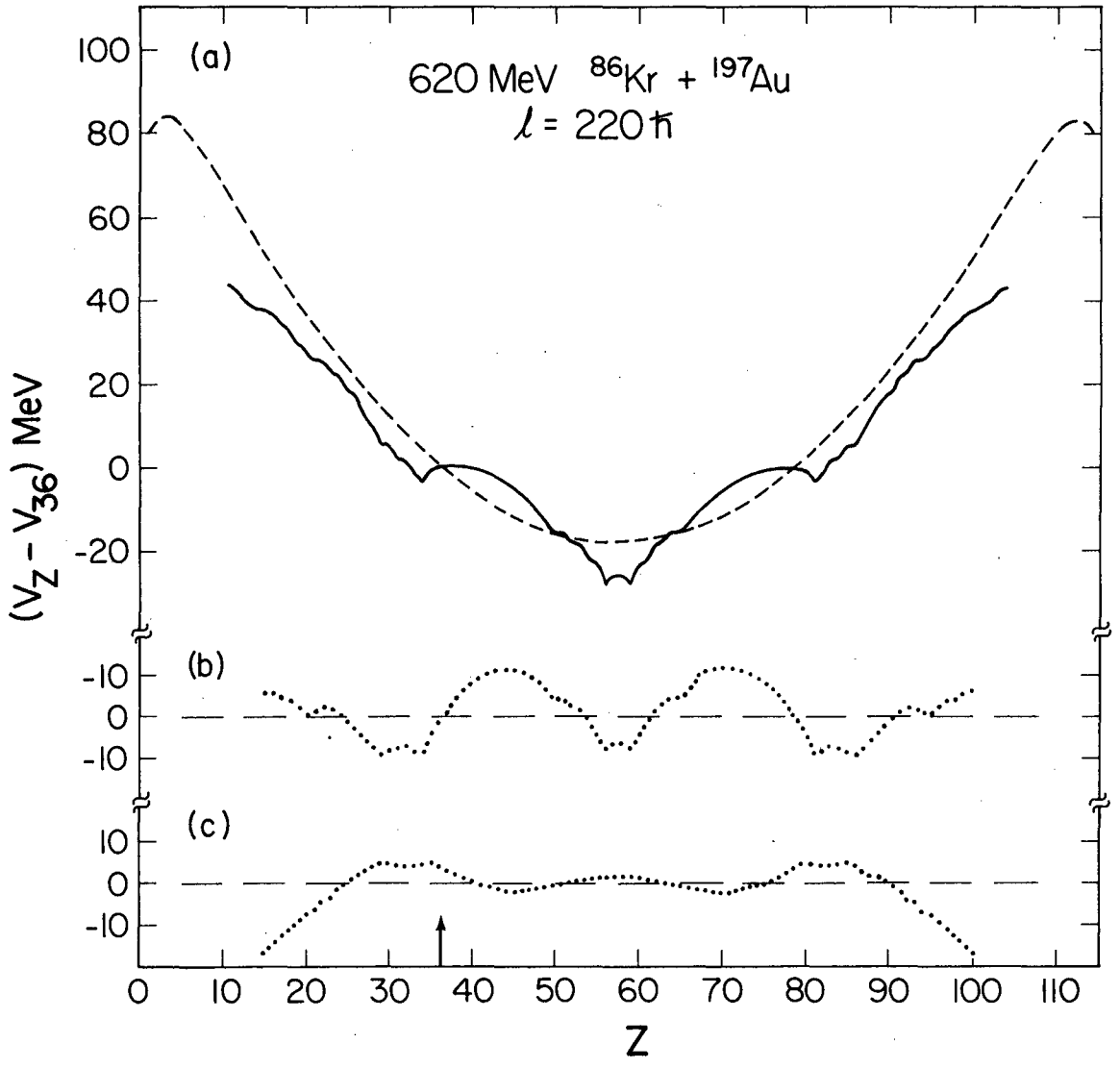

Fig. 4

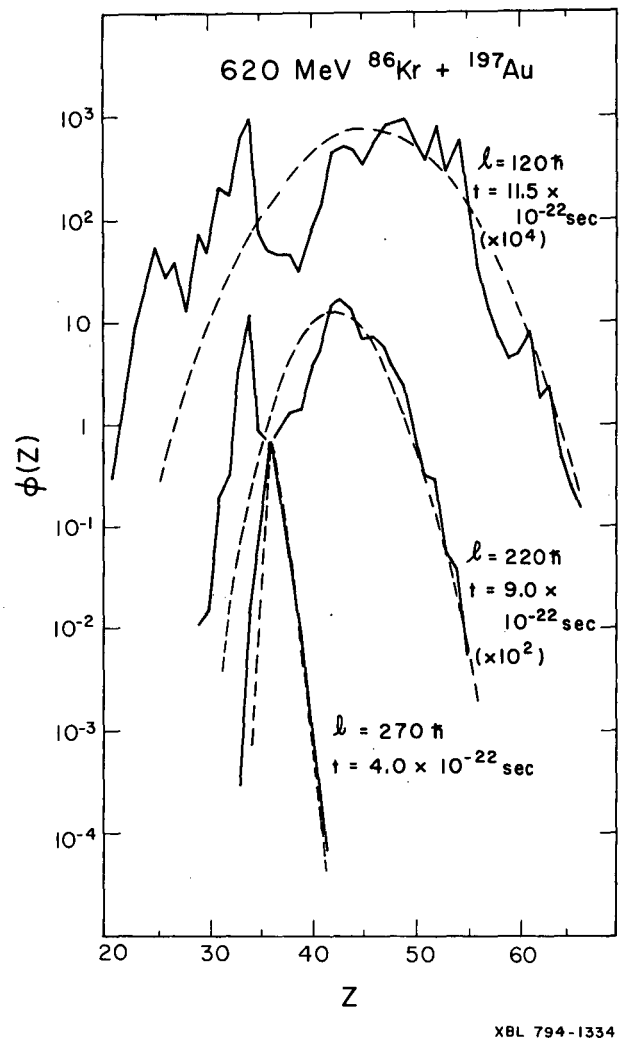
620 MeV ^{86}Kr + ^{197}Au
ℓ = 120 ħ
t = 11.5 x 10^{-22} sec
(x10^4)
ℓ = 220 ħ
t = 9.0 x 10^{-22} sec
(x10^2)
ℓ = 270 ħ
t = 4.0 x 10^{-22} sec
ϕ(Z)
Z
XBL 794-1334

Fig. 5

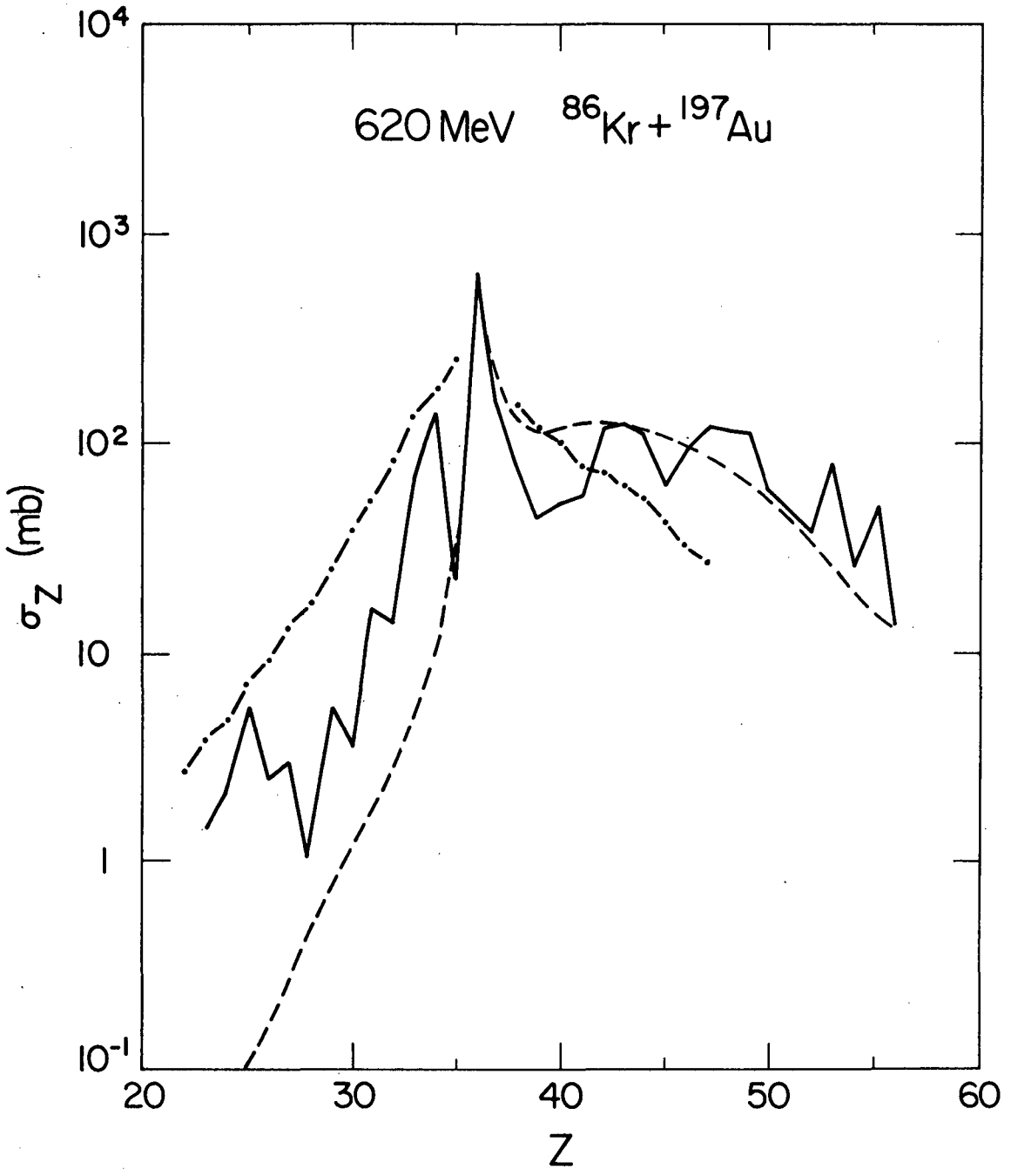

XBL 794-1333

Fig. 6

TECHNICAL INFORMATION DEPARTMENT
LAWRENCE BERKELEY LABORATORY
UNIVERSITY OF CALIFORNIA
BERKELEY, CALIFORNIA 94720